Lysosomal acid lipase-deficient mice: depletion of white and brown fat, severe hepatosplenomegaly, and shortened life span

Hong Du,[1,*] Martin Heur,[*] Ming Duanmu,[2,*] Gregory A. Grabowski,[*] David Y. Hui,[§] David P. Witte,[†] and Jaya Mishra[*]

Divisions of Human Genetics* and Pathology,† Children's Hospital Research Foundation, Cincinnati, OH, 45229; and Department of Pathology and Molecular Medicine,§ University of Cincinnati, College of Medicine, Cincinnati, OH 45267

Abstract **Lysosomal acid lipase (LAL) is essential for the hydrolysis of triglycerides (TG) and cholesteryl esters (CE) in lysosomes. A mouse model created by gene targeting produces no LAL mRNA, protein, or enzyme activity. The *lal*−/− mice appear normal at birth, survive into adulthood, and are fertile. Massive storage of TG and CE is observed in adult liver, adrenal glands, and small intestine. The age-dependent tissue and gross progression in this mouse model are detailed here. Although *lal*−/− mice can be bred to give homozygous litters, they die at ages of 7 to 8 months. The *lal*−/− mice develop enlargement of a single mesenteric lymph node that is full of stored lipids. At 6–8 months of age, the *lal*−/− mice have completely absent inguinal, interscapular, and retroperitoneal white adipose tissue. In addition, brown adipose tissue is progressively lost. The plasma free fatty acid levels are significantly higher in *lal*−/− mice than age-matched *lal*+/+ mice, and plasma insulin levels were more elevated upon glucose challenge. Energy intake was also higher in *lal*−/− male mice, although age-matched body weights were not significantly altered from age-matched *lal*+/+ mice. Early in the disease course, hepatocytes are the main storage cell in the liver; by 3–8 months, the lipid-stored Kupffer cells progressively fill the liver. The involvement of macrophages throughout the body of *lal*−/− mice provide evidence for a critical nonappreciated role of LAL in cellular cholesterol and fatty acid metabolism, adipocyte differentiation, and fat mobilization.**—Du, H., M. Heur, M. Duanmu, G. A. Grabowski, D. Y. Hui, D. P. Witte, and J. Mishra. **Lysosomal acid lipase-deficient mice: depletion of white and brown fat, severe hepatosplenomegaly, and shortened life span. *J. Lipid Res.* 2001.** 42: **489–500.**

Supplementary key words Wolman disease • cholesteryl ester storage disease • fatty liver

Lysosomal acid lipase (LAL; EC 3.1.1.13) is the enzyme that hydrolyzes cholesteryl esters (CE) and triglycerides (TG) that are delivered to lysosomes via the low density lipoprotein (LDL) receptor, LDL receptor-related protein, or other proteins and receptor(s) (1–4). The products of LAL hydrolysis including cholesterol, di- and monoacylglycerides, and free fatty acids are transported to the cytoplasm for re-esterification, storage, membrane biogenesis, steroid hormone production, bile acid synthesis, or energy provision. Cholesterol egress from the lysosomes increases the cytoplasmic cholesterol pool and triggers important regulatory steps: *1*) suppression of 3-hydroxy-3-methylglutaryl coenzyme A (HMG-CoA) reductase activity, the rate-limiting step in cholesterol syntheses; *2*) down-regulation of LDL receptors and HMG-CoA reductase mediated by the sterol regulated transcription factors, sterol regulatory element binding protein (SREBP)-1 and SREBP-2, which leads to a decreased delivery of lipoprotein-bound CE into the lysosomal compartment; and *3*) activation of acyl CoA:cholesterol acyltransferase leading to intracytoplasmic resynthesis of CE. These findings indicate a central role for LAL in the homeostasis of cellular cholesterol and fatty acids.

Deficiency of LAL is associated with two phenotypes in humans: Wolman disease (WD) and CE storage disease (CESD). WD is a severe infantile-onset phenotype resulting in death usually in the first year of life. These patients have massive storage of CE and TG in liver and small intestine, and become cachectic from malabsorption (5). CESD, a milder later-onset variant, is characterized by predominant CE deposition in many visceral tissues, al-

Abbreviations: BAT, brown adipose tissue; CE, cholesteryl ester; CESD, cholesteryl ester storage disease; FPLC, fast phase liquid chromatography; GFAP, glial fibrillary acidic protein; HMG-CoA, 3-hydroxy-3-methylglutaryl coenzyme A; LAL, lysosomal acid lipase; LDL, low density lipoprotein; ORO, oil red O; PBS, phosphate-buffered saline; TG, triglycerides; VLDL, very low density lipoprotein; WAT, white adipose tissue; WD, Wolman disease

[1] To whom correspondence should be addressed.
e-mail: duh0@chmcc.org

[2] Current address: Cell Biology Laboratory, Salk Institute for Biological Studies, La Jolla, CA 92037.

though hepatomegaly may be the only clinical manifestation. CESD patients can survive beyond middle age (5).

The mouse and human enzymes are encoded by ~3.2-kb and ~2.5-kb cDNA with 75% identity and 95% similarity of the deduced amino acid sequences (6, 7). The human and mouse LAL genes encompass 10 exons spanning 37 and 47.7 kb of genomic DNA with the same exon/intron organization (8, 9). The human LAL gene was mapped to chromosome 10q23.2-23.3 (10). The expression patterns of mouse LAL mRNA and protein are in a similar distribution to the tissue involvement in WD; that is, high-level expression was found in liver parenchymal cells and Kupffer cells, splenic macrophages, epithelial cells of the small intestine, the two inner layers of the adrenal cortex (zona fasciculata and zona reticularis), and renal tubular epithelial cells (6). The expression of mouse LAL in heart and skeletal muscle cells was low.

We used gene targeting by homologous recombination to develop a mouse model that mimics WD and CESD (11). The initial characterization of *lal*−/− mice demonstrated no LAL mRNA, protein, or enzyme activity. The *lal*−/− mice appear normal at birth and survive into adulthood. However, massive accumulations of TG and CE in liver, spleen, and small intestine were found.

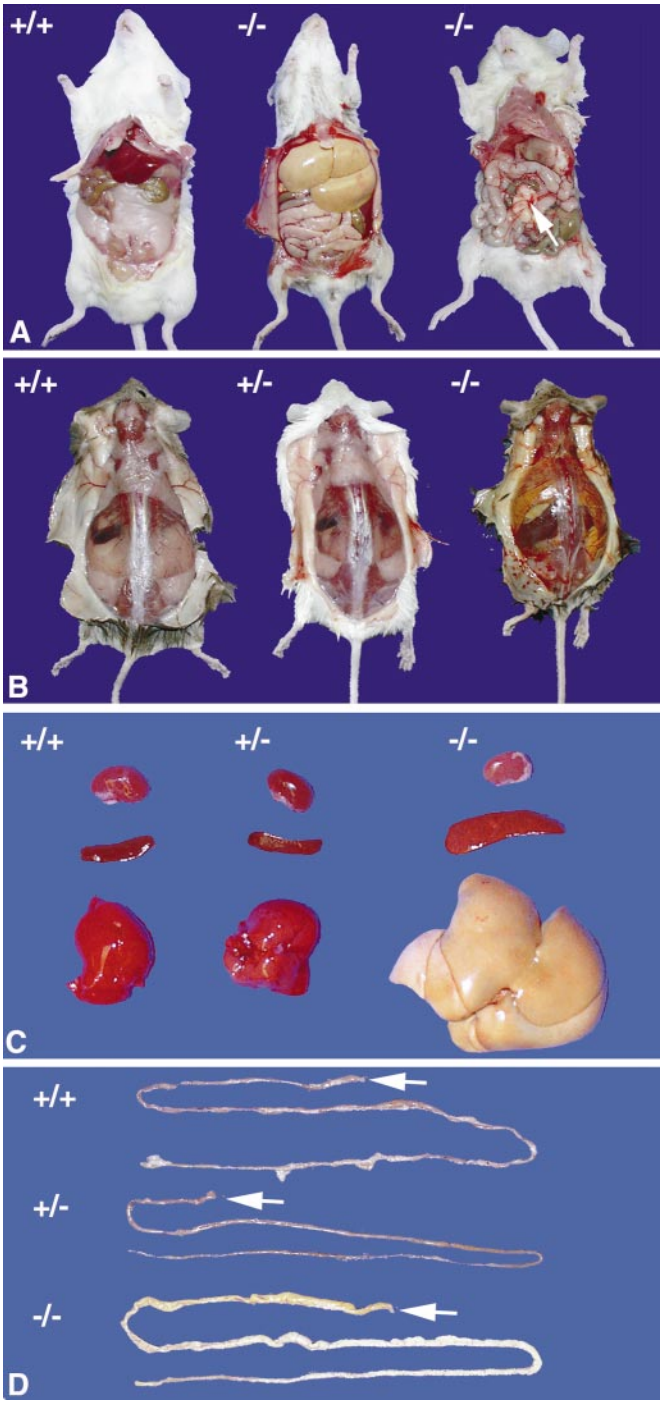

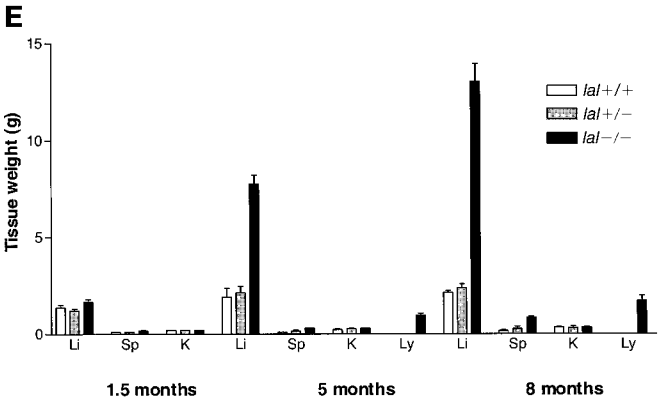

Fig. 1. Photographs of 6-month *lal*+/+ (left) and *lal*−/− (middle and right) littermate mice. A: A ventral view illustrates the enlarged fatty liver and absence of white adipose tissue (WAT) in a knockout mouse (middle) compared with the wild-type mouse (left). A unique large lymph node was observed only in elder-affected mice (right, indicated by arrow). B: A dorsal view illustrates the lack of brown adipose tissue (BAT) in the knockout mouse (right) compared with *lal*+/+ (left) and *lal*+/− (middle) mice. C: Gross appearance of liver, spleen, and kidney from 6-month *lal*+/+ (left), *lal*+/− (middle), and *lal*−/− (right) mice. D: Gross appearance of intestines from 6-month mice with *lal*+/+, *lal*+/−, and *lal*−/− genotypes. The arrow indicates the direction of duodenum to jejunum. E: Comparison of age-dependent hepatosplenomegaly. Average of five mice in each genotype and age group was presented. Li, liver; Sp, spleen; K, kidney; Ly, lymph node.

In this article, the progressivity of tissue and gross involvement of *lal*−/− mice is presented. A paucity of white adipose tissue (WAT) and brown adipose tissue (BAT) was present in *lal*−/− mice early in life, but these two forms of TG depots virtually disappeared by 6–8 months. This was concomitant with progressive Kupffer cell CE and TG storage. In addition, the physiological consequence of lost WAT and BAT in *lal*−/− mice was shown as similar to lipoatrophic diabetes. This progression phenotype in *lal*−/− mice provides evidence for critical roles of LAL in cellular lipid metabolism, adipocyte differentiation, and fat mobilization.

METHODS

Animals

Care and treatment practices of mice were in accordance with institutional guidelines, and all procedures were in accordance with IACUC-approved protocols at the Children's Hospital Research Foundation. The *lal*−/− mice originated from mixed genetic backgrounds of 129Sv and CF-1. Mice were housed in microisolation, under 12-h dark/light cycles. Water and food (regular chow diet) were available ad libitum. The mice were genotyped by polymerase chain reaction-based screening of tail DNA (11).

Plasma lipids

Blood was collected from the inferior vena cava of all overnight-fasting mice after they were anesthetized with the triple sedative (Ketamine, Acepromazine, and Xylazine). Plasma was collected by centrifugation of blood at 5,000 *g* (10 min, 4°C) and stored (4°C and −20°C). Plasma free cholesterol, total cholesterol, TG, and free fatty acid concentrations were determined by colorimetric kit assays (COD-PAP kit for free cholesterol and ACS-ACOD kit for free fatty acid were from Wako Chemicals, Kyoto, Japan; Triglycerides/GB kit and Cholesterol/HP kit were from Boehringer).

Plasma glucose and insulin determination

Nonfasting mice were bled through retro-orbital plexus before glucose load, and then glucose (3 g/kg) was injected intraperitoneally. Plasma samples were collected again 30 min postglucose injection. Plasma glucose was determined using glucose HK kit (Sigma), and plasma insulin was determined using rat insulin radioimmunoassay kit (Linco Research).

Lipoprotein analyses

Plasma samples (200 μl) were subjected to fast phase liquid chromatography (FPLC) gel filtration on two Superose 6 HR columns (Pharmacia Biotech Inc.) as described (12). Each fraction (0.5 ml) was collected, and cholesterol concentrations were determined (Cholesterol/HP kit from Boehringer).

Histological analyses

Light microscopic examinations of most organs were conducted after the sections were stained with hematoxylin/eosin (paraffin-embedded) or oil red O (ORO; frozen sections). For electron microscopic analysis, liver tissue samples were fixed in 3% gluteraldehyde in cacodylate buffer, post-fixed in 1% osmic acid, and embedded in LX resin (Ladd Research Industries, Burlington, VT); ultra-thin sections stained with lead uranyl acetate were examined with a Zeiss EM912 electron microscopy.

Immunohistochemical staining

Antibodies used in this study were rat anti-bovine serum albumin (anti-BSA; Cal Biochem), goat anti-mouse Desmin and goat anti-mouse glial fibrillary acidic protein (GFAP, Santa Cruz), and rat anti-mouse F4/80 (Serotec). Immunohistochemical staining with paraffin-embedded liver sections was performed with all antibodies, except for F4/80. For immunohistochemical staining of F4/80, a fixative with 2% paraformaldehyde, lysine, and periodate was used as described (13). Postfixative procedures are identical for all antibody staining. The primary antibody was incubated at 4°C overnight using the dilution as suggested by the manufacturer. The sections were then washed with PBS (three times, 5 min/wash), incubated with Biotin-conjugated secondary antibody (1:100 dilution) for 30 min at room temperature, and washed with PBS (5 min). The secondary antibody was either goat anti-rat IgG or donkey anti-goat IgG (Vector). The signal was detected using VECTASTAIN ABC kit (Vector) and counterstained with Nuclear Fast Red.

Tissue lipid analyses

Total lipids were extracted from liver, spleen, and small intestine by the Folch method (11, 14). TG concentrations were quantified as described (15). Total tissue cholesterol concentrations were measured using o-phthalaldehyde (16).

RESULTS

Progressive hepatosplenomegaly

With age, *lal*−/− mice showed progressive hepatosplenomegaly. The average liver weight of age-matched *lal*−/− mice compared with wild-type mice was ~1.2-fold at 1.5 months (n = 5), ~4.1-fold at 5 months (n = 5), and ~6.2-fold at 7.5–8 months (n = 7; **Fig. 1A, C**, and **E**). These values represent, respectively, 8.2%, 22.4%, and 35.1% of body weight (BW; **Table 1**). The liver weights of heterozygous mice were comparable to those of wild-type mice (Table 1). Splenomegaly in *lal*−/− mice was first observed at the age of 3 months (data not shown), with progression to 4.4-fold greater than that of age-matched wild-type mice by 8 months (Table 1). The heterozygous mice did not show splenomegaly. The kidney in *lal*−/− mice was of

TABLE 1. Progressive hepatosplenomegaly

	Liver Weight/Body Weight(%)			Spleen Weight/Body Weight (%)		
Genotype	1.5 months	5 months	8 months	1.5 months	5 months	8 months
lal+/+ (n = 5)	6.4 ± 1.2	4.8 ± 0.5	5.0 ± 0.6	0.47 ± 0.03	0.38 ± 0.05	0.47 ± 0.03
lal+/− (n = 5)	6.2 ± 0.5	5.4 ± 1.1	4.9 ± 1.1	0.51 ± 0.01	0.43 ± 0.12	0.44 ± 0.07
lal−/− (n = 7)	8.2 ± 0.5	22.4 ± 2.1	35.1 ± 2.3	0.81 ± 0.19	0.87 ± 0.09	2.06 ± 0.46

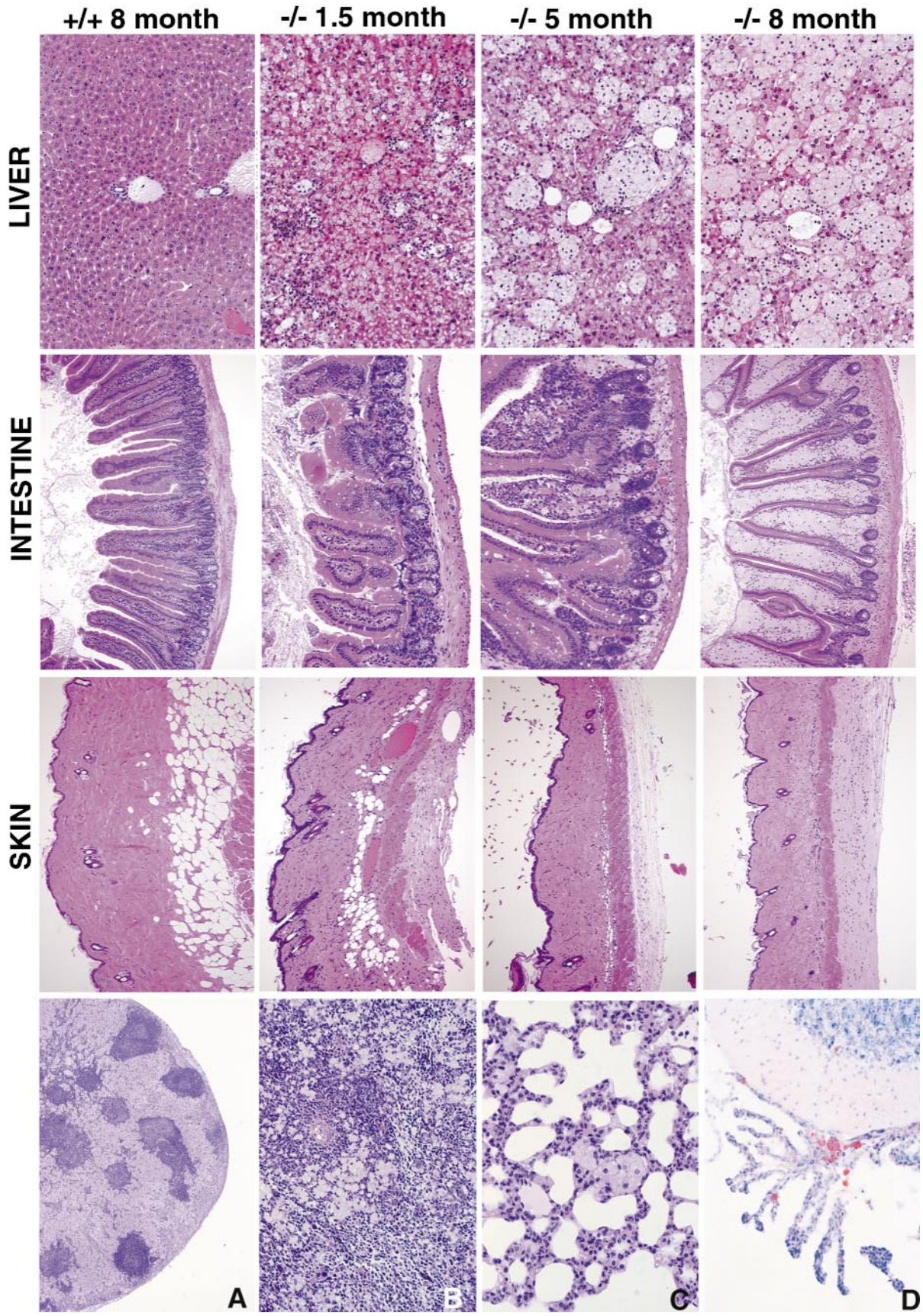

Fig. 2.

normal weight, but was noticeably paler than those from *lal*+/+ and *lal*+/− mice (Fig. 1C).

Enlargement of the mesenteric lymph node in *lal*−/− mice

At 2 months, *lal*−/− mice developed an enlarged mesenteric lymph node (Fig. 1A). Histologic analyses showed a lymphoid and macrophage character (**Fig. 2A**) with a weight of 0.98 ± 0.5 g (n = 13) at 8 months. The enlargement of the lymph node was due to lipid storage in macrophages rather than lymphocyte proliferation. The largest node was 2.5 g. This mesenteric lymph node was not present in *lal*+/+ and *lal*+/− mice at the gross level.

Absence of WAT and BAT in *lal*−/− at 6 months

The *lal*−/− mice completely lacked inguinal, interscapular, and retroperitoneal WAT at 6 months (Fig. 1A and B). A small amount of epididymal fat was present, but this was much less than that of age-matched wild-type mice. Also, *lal*−/− mice at 6 months did not have BAT in gross level (Fig. 1B), although the BAT was presented at 1 month in *lal*−/− mice (data not shown). Because BAT is critical for nonshivering thermogenesis in small mammals and younger large mammals (17), nonstressed and stressed (4°C for 12 h) core body temperature was evaluated in age-matched *lal*+/+ and *lal*−/− mice. No significant difference was found (data not shown). To investigate the etiology of the lack of WAT, skin samples were isolated from corresponding areas of age-matched *lal*+/+ and *lal*−/− mice. Subcutaneous WAT was present in *lal*−/− mice at 1.5 months, but with a significantly decreased number of adipocytes. Subcutaneous WAT was greatly diminished at 5 months, and was undetectable at 8 months (Fig. 2, skin). The subcutaneous adipocyte size was similar in *lal*+/+ and *lal*−/− mice at 1.5 months (data not shown).

Histologic analyses

Hepatocytes had significant vacuolation and neutral lipid storage at 1.5 months. By light microscopy with increasing age, the percentage of storage cells that were hepatocytes decreased (Fig. 2, liver) and ~40% of ORO-positive cells were nonhepatocytes by 5 months and ~85% by 8 months (data not shown). These resembled hypertrophic and hyperplastic Kupffer cells (see below).

To positively identify the cell type responsible for the massive lipid accumulation in *lal*−/− mice at 5 to 8 months, immunofluorescence staining with anti-BSA, which cross-reacts with mouse albumin, was performed. Hepatocytes stained positive for BSA, whereas the major lipid storage cells did not (**Fig. 3A**). Antibodies recogniz-

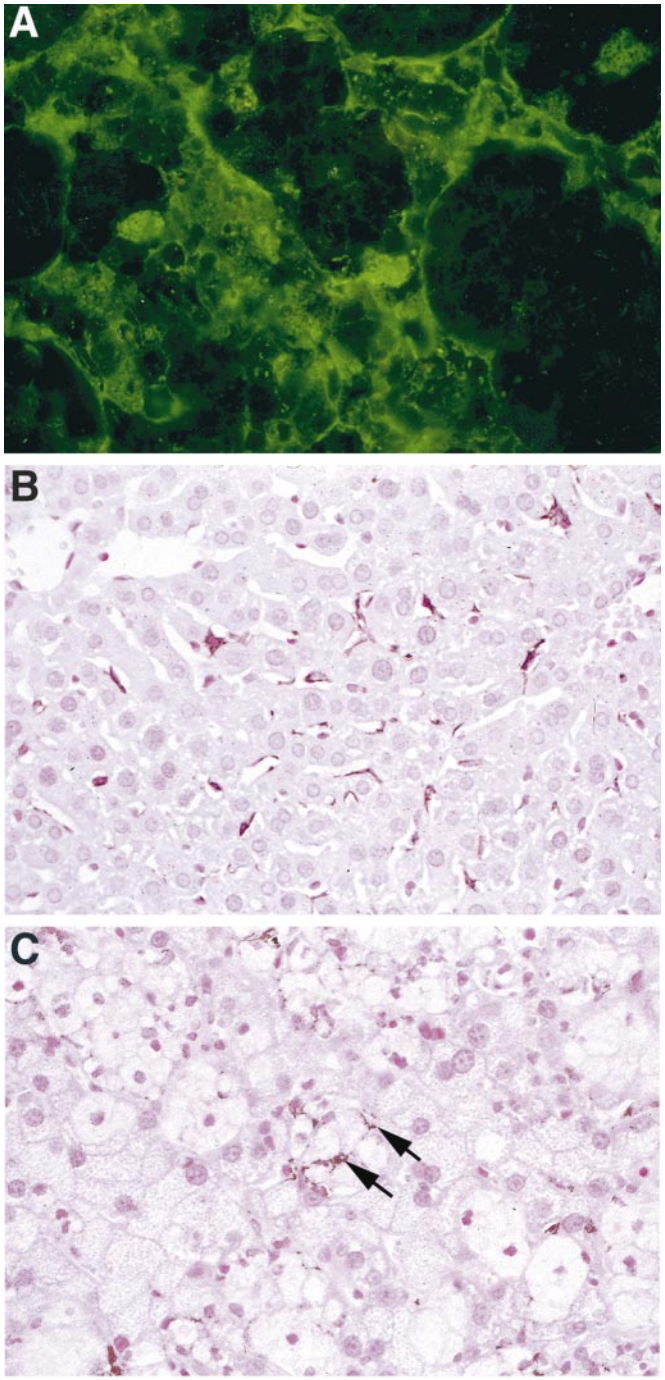

Fig. 3. Lipid storage cells in *lal*−/− mouse liver are nonhepatocytes. A: Immunofluoresecence staining of mouse albumin in liver section of 5-month *lal*−/− mouse. B and C: Immunohistochemical staining of macrophages specific antigen (F4/80) in liver section of *lal*−/− mice at 1 month (B) and 5 months (C). The arrows indicate the positive staining of F4/80, which is much weaker in 5-month *lal*−/− liver owing to lipid storage and probably expansion of cellular membrane.

Fig. 2. Histology of age-dependent lipid storage in liver and small intestine and age-dependent WAT disappearance. Hematoxylin/eosin (H&E) staining of paraffin-embedded sections from liver, small intestine, and skin from the back of an 8-month *lal*+/+ mouse, and 1.5-month, 5-month, and 8-month *lal*−/− mice as indicated. Notice that the lipids are mainly stored in hepatocytes in younger mice (1.5 months) and then in nonhepatocytes at the age of 5 and 8 months. The lipid accumulation in lamina propria is more significant at 5 months in the *lal*−/− mouse. At 8 months, the villi are swollen and full of lipid. Notice that the subcutaneous WAT are present in the younger *lal*−/− mouse, decrease significantly at 5 months, and completely disappear at 8 months. H&E staining of the enlarged lymph node (A), spleen (B), lung (C), and oil red O (ORO) staining of choroid plexus (D) from a 6-month *lal*−/− mouse.

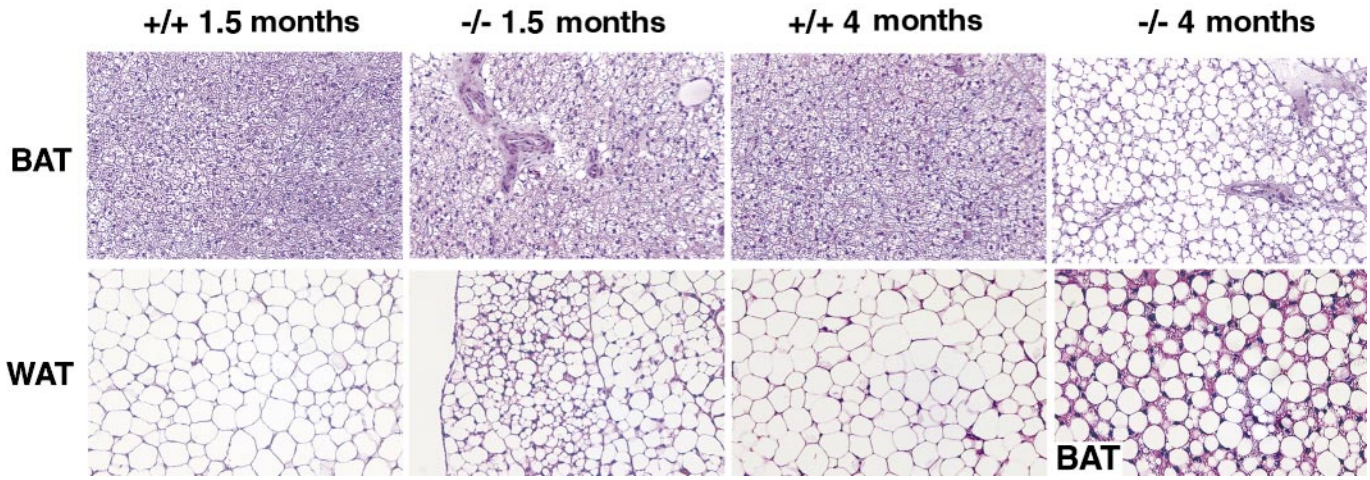

Fig. 4. Histologic comparison of BAT and WAT in *lal*+/+ and *lal*−/− mice at age 1.5 months and 4 months. H&E staining of paraffin-embedded sections of BAT and WAT from *lal*+/+ and *lal*−/− mice at 1.5 months and 4 months. Original amplification: 200×, except BAT from *lal*−/− at 4 months, at bottom: 400×.

ing macrophage-specific markers (anti-mouse Mac-1 or anti-mouse F4/80) and Ito cell markers (anti-desmin or anti-GFAP) were used to identify the nature of the storage cells. The lipid storage cells are negative for desmin, GFAP, and Mac-1 (data not shown) and positive for F4/80 (Fig. 3B and C). The intensity of F4/80 staining in lipid storage cells was much lower in liver at 5 months than that in the Kupffer cells of 1.5-month *lal*−/− mice (Fig. 3B and C). These results suggest that, owing to the excessive storage of lipids and increased cell volume, the expression

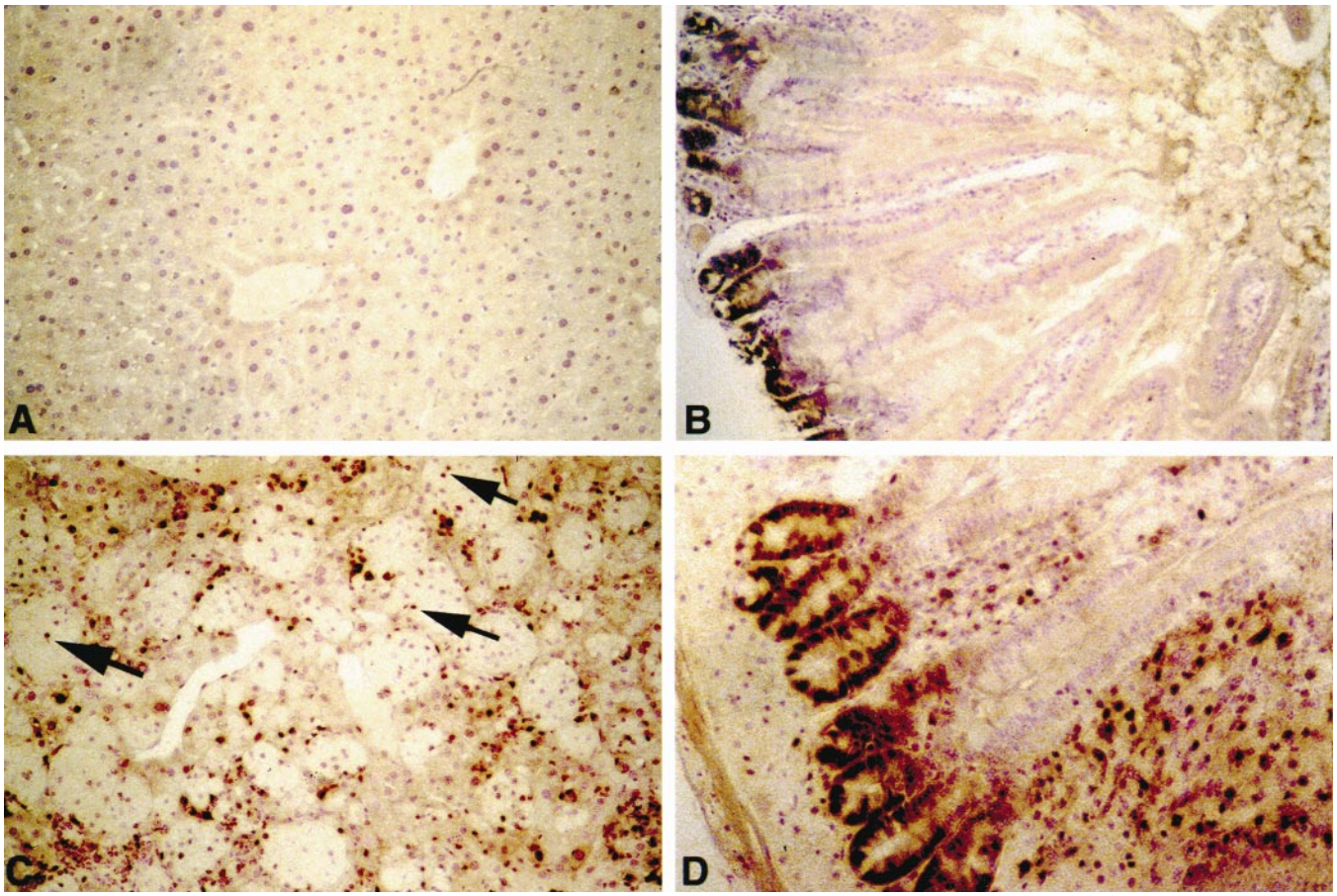

Fig. 5. Hepatocytes and Kupffer cells are proliferating in liver of *lal*−/− mice. Immunohistochemical staining of proliferating cell nuclear antigen in liver (A and C) and small intestine (B and D) sections. A and B are from *lal*+/+ mice, and C and D are from *lal*−/− mice. The arrows indicate positive staining of Kupffer cells.

of macrophage-specific makers might be diluted (due to increased surface area) or altered in these cells.

Histologically, BAT in *lal*−/− mice at 1.5 months was similar to that of age-matched *lal*+/+ mice. In comparison, WAT in *lal*−/− mice at 1.5 months was significantly diminished, and the adipocytes had considerable size heterogeneity compared with that of age-matched *lal*+/+ (**Fig. 4**). By 4 months, *lal*−/− mice had undetectable WAT. BAT in *lal*−/− mice at 4 months histologically resembled WAT (Fig. 4), with increased lipid droplet size in the cells. This result suggested a decrease of uncoupling proteins (UCP) in BAT of these *lal*−/− mice (23).

With increasing age, the small intestine became more discolored in a proximal to distal progression, with the duodenum being yellow and the jejunum being cream white (Fig. 1D). Histological analyses showed progressive lipid storage in lamina propria of intestinal villi in cells that were proliferated macrophages (see below). The amount of lipid stored in the small intestine was progressive with age (Fig. 2, intestine). At 6 months, the spleen had the accumulation of lipid storage cells (Fig. 2B). Additional tissues with lipid storage cells in the older *lal*−/− mice included macrophages in the lung (Fig. 2C) and the epithelial cells of the choroid plexus (Fig. 2D).

Proliferation of hepatocytes and Kupffer cells in *lal*−/− mice

To determine whether the lipid-stored Kupffer cells are accumulated due to recruitment from the circulation or proliferation in situ, immunohistochemical staining with antibody against proliferating cell nuclear antigen (PCNA) was performed with liver sections from *lal*+/+ and *lal*−/− mice at 5 months. Basal columnar cells in crypts of small intestine are the stem cells for villous and crypt epithelium. Cell division in basal column cells in crypts was confirmed by positive staining of PCNA (**Fig. 5B** and **C**). PCNA staining in liver section of *lal*+/+ was negative (Fig. 5A). Both hepatocytes and Kupffer cells (arrow in Fig. 5C) stained positively with PCNA in liver section of *lal*−/− mice (Fig. 5C). The lipid storage cells in the small intestine of *lal*−/− mice were also positive for PCNA staining (Fig. 5D). These results suggest that the storage cells in liver and small intestine were proliferating macrophages.

Ultrastructure of storage cells

To evaluate the intracellular location of the lipid stored in cells, electronic microscopic analyses were performed. Although some lipid droplets were free in cytoplasm, the majority of lipid was present within unit membrane vesicles, that is, lysosomes (**Fig. 6B**). CE crystals were also observed in the cytoplasm of storage cells (Fig. 6A).

Plasma lipid profiles

Plasma was collected and the lipid profiles were analyzed by FPLC fractionation and ORO staining after agarose gel electrophoresis of plasma. The *lal*−/− mice showed an increased level of LDL cholesterol by FPLC fractionation (**Fig. 7**) and the presence of β-migrating lipoproteins in agarose gels (insert of Fig. 7). A lower than normal high density lipoprotein (HDL) level was evident on FPLC migration profiles, and the *lal*−/− mice HDL had a faster mobility than that from normal mice by agarose electrophoresis. The total cholesterol levels in plasma of *lal*+/+ and *lal*−/− mice were not significantly different (7).

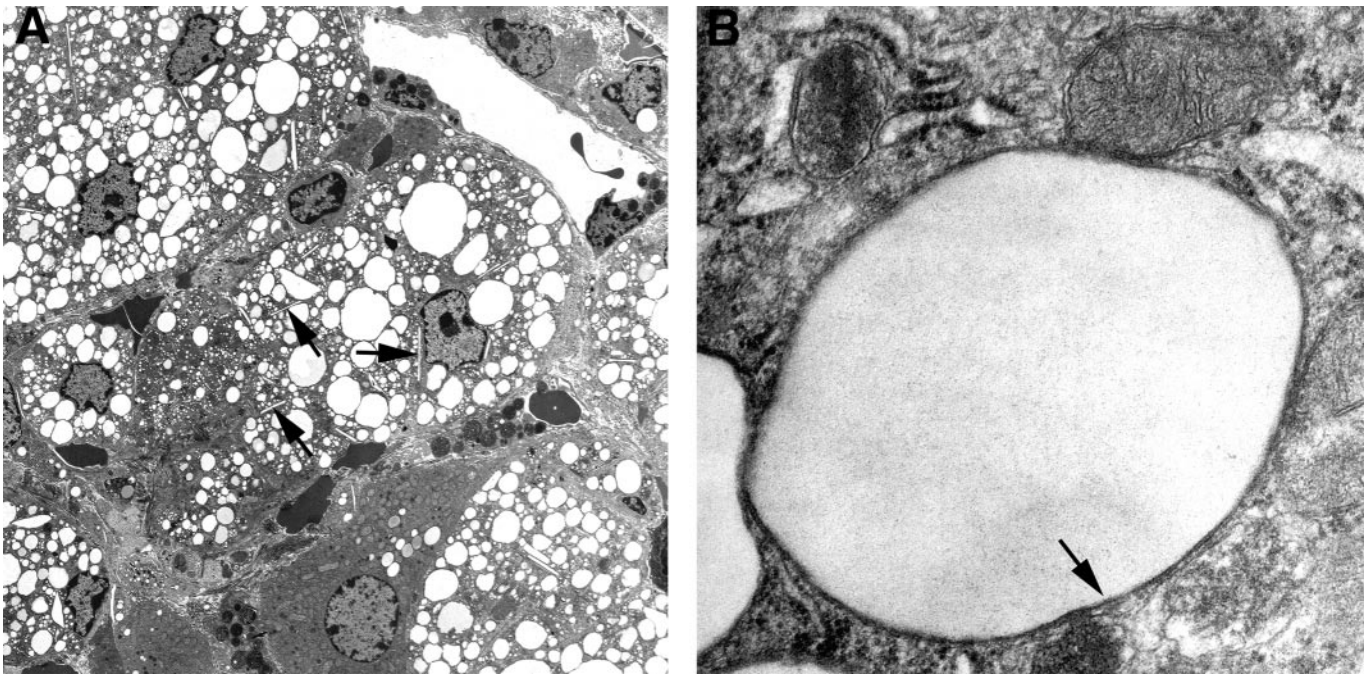

Fig. 6. Electronic microscopic analysis of subcellular localization of lipid storage from 6-month *lal*−/− mouse liver. The original magnifications are (A) 1250× and (B) 31,500×. The arrow indicates the accumulation of cholesterol crystal.

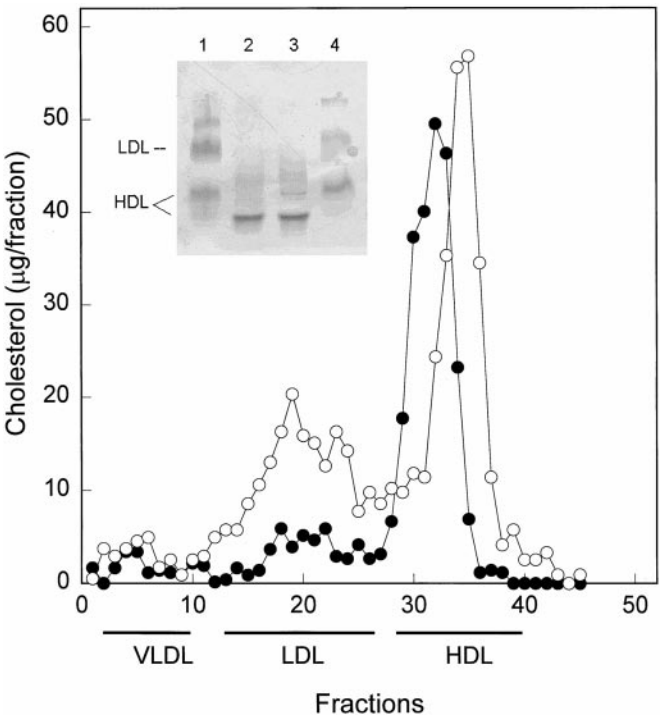

Fig. 7. Analysis of serum lipoproteins in *lal*+/+ and *lal*−/− mice. A total of 200 μl of mouse serum from *lal*+/+ (closed circle) or *lal*−/− (open circle) mice was applied to 2 fast protein liquid chromatography (FPLC) Superose 6 columns connected in series. Fractions (0.5 ml) were collected by elution with PBS containing 1 mM ethylenediaminetetraacetic acid. Cholesterol content in each fraction was analyzed with an enzymatic assay kit. The insert shows the agarose gel electrophoretic patterns of serum lipoproteins from *lal*−/− (lanes 1 and 4) and *lal*+/+ (lanes 2 and 3) mice. The FPLC elution profile and electrophoretic mobility of standard very low density lipoprotein (VLDL), low density lipoprotein (LDL), and high density lipoproteins (HDL) were included for comparison.

Tissue lipid storage

CE and TG amounts in tissues progressively increased with age. Compared with age-matched *lal*+/+, *lal*−/− livers showed increases of CE 14.7-fold at 1.5 months, 18.7-fold at 5 months, and 42.5-fold at 8 months (**Fig. 8A**). In spleen, these ratios were 3-fold at 1.5 months, 15.6-fold at 5 months, and 26.8-fold at 8 months (Fig. 8B). For total TG, *lal*−/− livers had increases of 4.9-fold at 1.5 months and 10-fold at 5 and 8 months (Fig. 8C). The *lal*−/− splenic TG increased from 3.1-fold at 1.5 months to 7.3-fold at 5 months and to 14.2-fold at 8 months (Fig. 8D). The *lal*−/− intestine stored more TG than cholesterol (compare Fig. 8E and F). The cholesterol and TG storage in intestine also showed age-dependent progression (Fig. 8E and F).

Energy intake and insulin resistance

Wild-type and *lal*−/− male mice had similar average BW (**Fig. 9A**). Interestingly, both male and female *lal*−/− mice had significant higher food intake compared with age-matched and BW-mated *lal*+/+ mice (Fig. 9B). To understand the etiology of fat transfer out from adipose tissue, the plasma nonesterified fatty acid (NEFA) and TG levels were measured from age-matched *lal*+/+ and *lal*−/− mice after overnight fasting. The plasma NEFA levels in *lal*−/− mice were significantly higher than *lal*+/+ mice at both 2 and 4 months of age (**Fig. 10A**). The plasma TG levels were not significantly different between *lal*+/+ and *lal*−/− mice (Fig. 10B).

Because most of the fatless mouse models developed an insulin-resistant phenotype, the plasma glucose and insulin levels were determined before and after a glucose load in *lal*−/− mice. The plasma glucose levels were lower in *lal*−/− mice before glucose load and showed no significant difference from *lal*+/+ mice after glucose load (Fig. 10C). However, the plasma insulin level was 6.7-fold higher in *lal*−/− than that in *lal*+/+ mice after glucose load for 30 min (Fig. 10D). This result indicated that *lal*−/− mice have significant insulin resistance.

DISCUSSION

This study provides insights into the progressive phenotype of *lal*−/− mice and establishes complete LAL deficiency as primarily a macrophage disease. Absence of LAL produces significant changes in fatty acid mobilization, adipocyte differentiation, insulin sensitivity, and in the shift of lipid storage from hepatocytes to Kupffer cells. The progressive phenotypic involvement shows major effects on body energy metabolism and indicates that the liver macrophages are directly involved in overall cholesterol and TG metabolism.

A unique characteristic of the *lal*−/− mouse is the hypertrophy and hyperplasia of macrophages. This was particularly evident in the liver with engorged Kupffer cell accumulation. This was also identified in the LAL-deficient rat and in human patients with WD or CESD (5, 18). These findings contrast with other lysosomal storage diseases (e.g., Gaucher disease and β-glucuronidase deficiency). In those diseases, only hypertrophy and accumulation of substrate-filled macrophages were shown (19). Another interesting aspect of this mouse *lal*−/− model is the initial (1.5 months) lipid storage in hepatocytes with a switch to predominantly Kupffer cell storage by 5–8 months. This shift in storage cell type was accompanied by hypertrophy and hyperplasia of Kupffer cells. Immunohistochemical staining of liver sections with anti-PCNA antibody showed positivity of hepatocytes and Kupffer cells of *lal*−/− mice at 5 months (Fig. 4). Wild-type mice were negative with this stain, indicating lack of significant cell division. Preliminary studies with mRNA from *lal*+/+ and *lal*−/− livers showed increased levels of monocyte colony stimulation factor (M-CSF) in *lal*−/− mice at 1 and 6 months (20). The increased expression of M-CSF could be a key factor for Kupffer cell proliferation in *lal*−/− liver because it is a major factor for monocyte to macrophage differentiation and proliferation (21, 22).

Fatty livers occur in other genetically modified mice [e.g., in transgenic mice with overexpression of the domi-

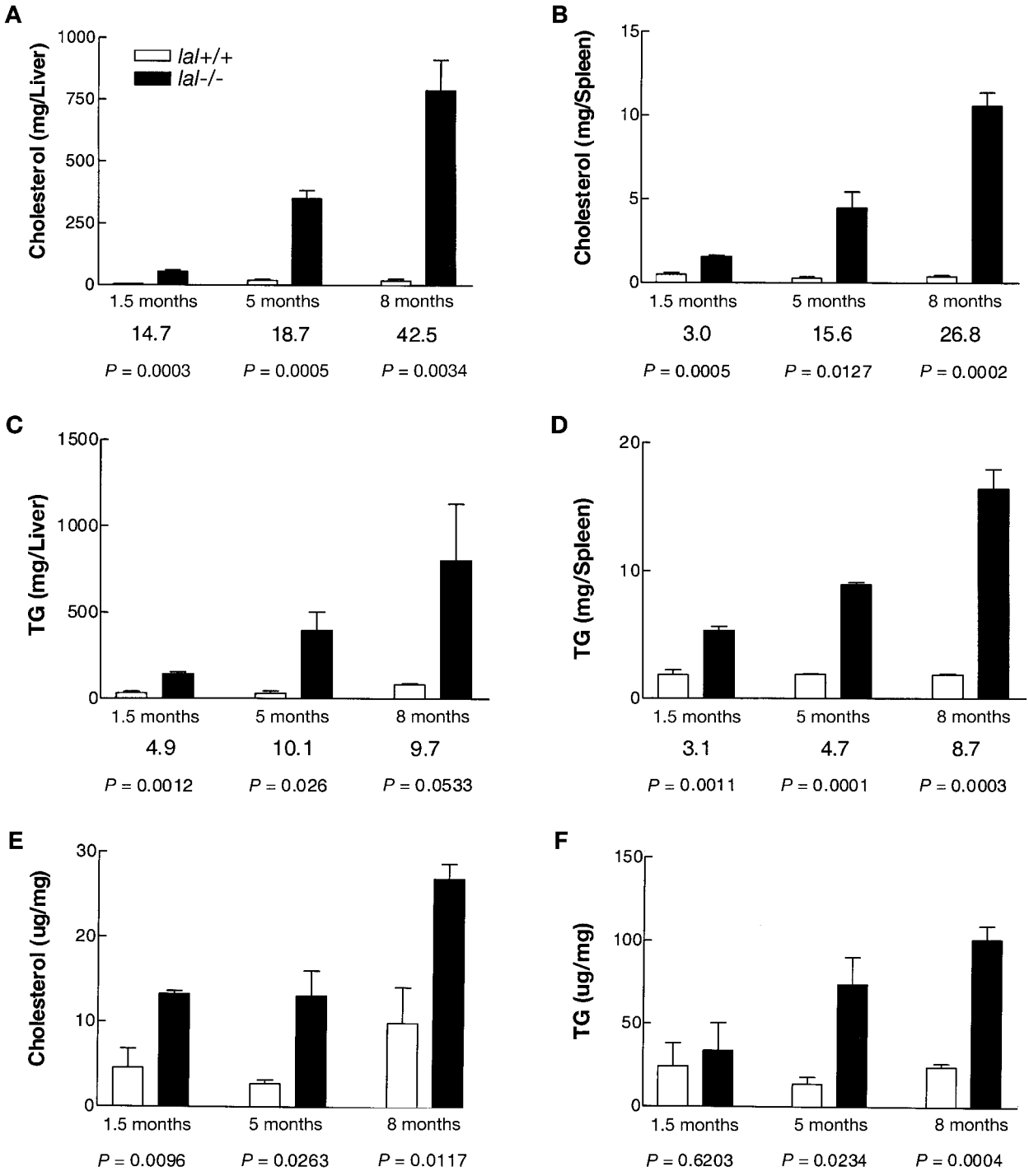

Fig. 8. Comparison of the tissue lipid at different ages. A: Total cholesterol per liver of *lal*+/+ and *lal*−/− mice at different ages. B: Total cholesterol per spleen of *lal*+/+ and *lal*−/− mice at different ages. C: Total triglycerides (TG) per liver of *lal*+/+ and *lal*−/− mice at different ages. D: Total TG per spleen of *lal*+/+ and *lal*−/− mice at different ages. E: Cholesterol concentration in small intestine of *lal*+/+ and *lal*−/− mice at different ages. F: TG concentration in small intestine of *lal*+/+ and *lal*−/− mice at different ages. The increase fold of lipid between *lal*+/+ and *lal*−/− at each age group is shown. The *P* value refers to average tissue lipid amount between *lal*+/+ and *lal*−/− at each age group.

nant positive fragment of N-terminal SREBP-1a (a.a 1-460)] (23), in LXRα knockout mice (24), and in the tetraploid-rescued PPARγ knockout mice (25). TG and cholesterol accumulate in the liver (~12% BW) of SREBP-1a460 transgenic mice (14.6-fold and 5.5-fold excess, respectively) (23). In comparison, only cholesterol accumulated (~8.5-fold) in liver (~9.5% BW at 3 months of age) of LXRα knockout mice compared with age-matched wild-type mice when on a cholesterol challenge diet (24). The *lal*−/− mice had more massive liver enlargement (35.1%

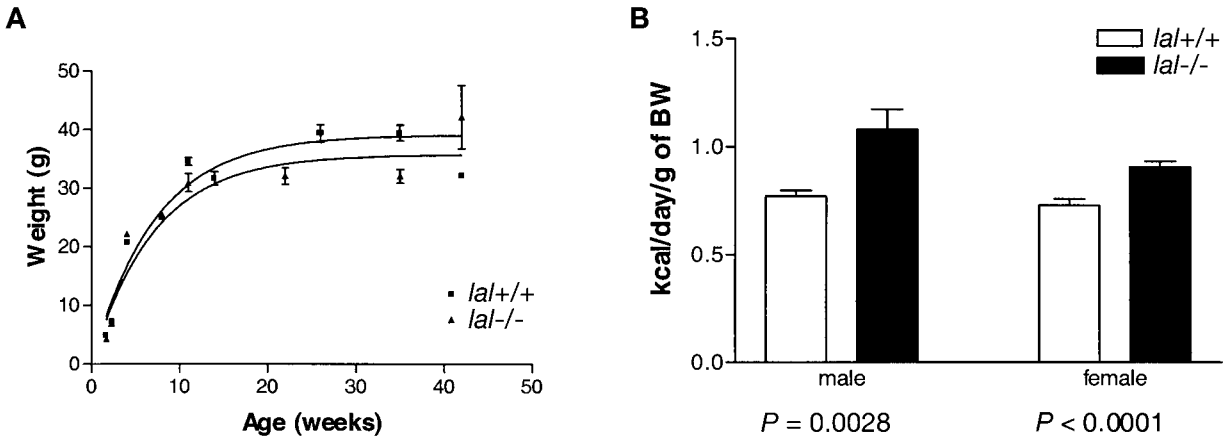

Fig. 9. Body weight (BW) and food intake of *lal*+/+ and *lal*−/− mice. A: BW of male mice (n = 6 for both *lal*+/+ and *lal*−/−). B: Food intake of *lal*+/+ and *lal*−/− mice at age 4 months (n = 5 for *lal*+/+ and n = 6 for *lal*−/−).

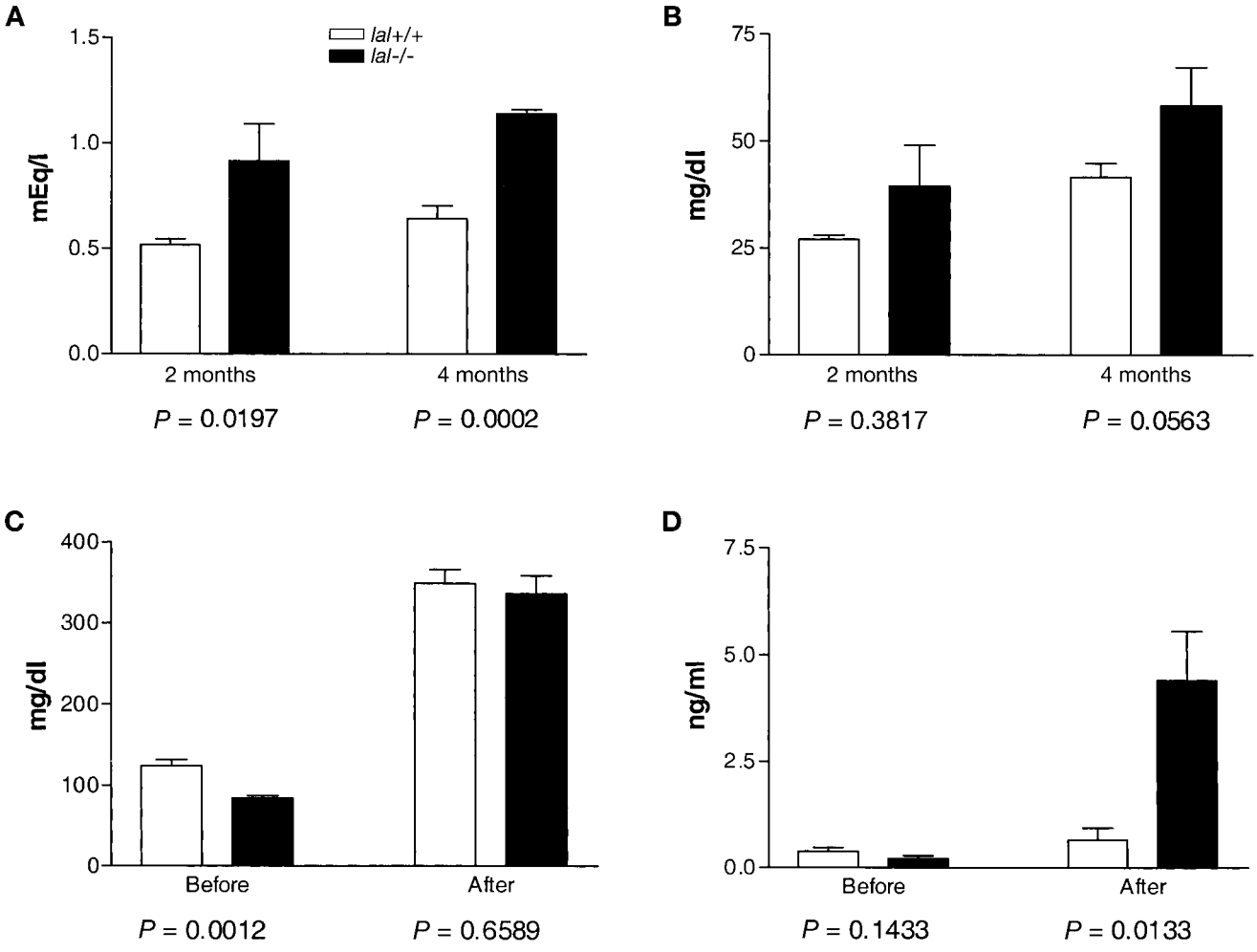

Fig. 10. Plasma nonesterified fatty acid (NEFA), TG, glucose, and insulin levels. Overnight fasting plasma samples were obtained and NEFA (A), and TG (B) were determined with commercially available kits (n = 5 for both *lal*+/+ and *lal*−/− at both 2- and 4-month age groups). Nonfasting plasma samples were collected before and after glucose loading (3 g/kg by ip injection) for 30 min. Plasma glucose levels (C) were determined by commerically available kit, and plasma insulin levels (D) were determined by rat insulin radioimmunoassay kit (Linco; n = 8).

BW at 8 months) and larger accumulations of TG and cholesterol (Fig. 8A and C). The common characteristic of these fatty liver mice is a disruption of cholesterol and fatty acid homeostasis. SREBP-1a, LXRα, and PPARγ are transcription factors (26, 27). SREBP-1 regulates expression of multiple enzymes and proteins in the cholesterol and fatty acid synthetic pathways and in cholesterol uptake (26, 27). LXRα binds oxysterols and up-regulates cholesterol 7 α-hydroxylase (Cyp7a), the rate-limiting enzyme in bile acid synthesis (28). PPARγ is critical to adipose tissue differentiation. Interestingly, activation of these three transcription factors is dependent on intracellular cholesterol levels (for SREBP-1), oxysterols (for LXRα), or metabolites of fatty acids (for PPARγ) (29, 30). LAL is a critical enzyme for the release of these ligands from lysosome, which may explain the greater severity of phenotype in *lal*−/− mice compared with mice having disruption or overexpression of lipid metabolism-related transcription factors. These data also suggest a prominent role for LAL in cholesterol and fatty acid homeostasis relative to other cellular lipases.

The plasma cholesterol and TG levels in *lal*−/− mice are normal. This is in agreement with plasma lipid levels in WD, although CESD patients appear to have hypercholesterolemia (5). Variable increases in very low density lipoprotein (VLDL) cholesterol, as we detected in *lal*−/− mice, also are present in human CESD (5). The plasma lipid levels in *lal*−/− mice indicated that LAL might not play any major role in the plasma lipid homeostasis.

The loss of WAT and BAT in the *lal*−/− mice was unexpected. Age-dependent depletion of WAT in *lal*−/− mice also differs from other obesity-resistant transgenic mouse models in that the WAT were not totally depleted and the size of adipocytes was smaller than that of the wild-type control. Obesity-resistant transgenic mice include those with transgenes expressed under the control of the adipocyte lipid-binding protein (aP2) promoter of mitochondria UCP-1 (31) and β1-adrenergic receptor (32). Genetic leanness resulted from several other knockouts in mice, including C/EBPα−/−, a basic leucine zipper transcription factor α (33); GLUT4−/−, an insulin-sensitive glucose transporter (34); and RIIβ−/−, the regulatory subunit isoform IIβ of cAMP-dependent protein kinase A (35). More recently, two other fatless mice resulted from transgenic expression of the dominant active form of SREBP-1c or dominant-negative form of C/EBPα (called A-ZIP/F-1) under control of the aP2 enhancer/promoter. Both SREBP-1 and C/EBPα are key transcriptional factors that control the differentiation of WAT. The histology of these transgenic mice showed hepatocellular lipid accumulation, a mixture of mature and immature WAT adipocytes that varied widely, and BAT resembling WAT, lacking expression of UPC-1 (23). Size heterogeneity of adipocytes in WAT of *lal*−/− (1.5 months) and WAT-like cells in BAT of *lal*−/− mice (4 months) resemble the histologic observations in A-ZIP/F-1 mice, although the fatty liver is much more severe in *lal*−/− mice (22.4% of BW at 5 months) compared with age-matched A-ZIP/F1 mice (9.51% of BW at 5 months). Unlike A-ZIP/F1 mice, *lal*−/− mice are only slightly insulin resistant, and they are not diabetic. On the basis of the elevated plasma NEFA and increased expression of CD36 mRNA (H. Du et al., unpublished observations), it would be interesting to see whether double knockout of *lal*−/− and CD36−/− will reduce the fat mobilization and fatty liver in *lal*−/− mice. Availability of this *lal*−/− mouse model will allow us to further study the mechanism and the connection of adipose tissue differentiation and fat mobilization.

We thank Lisa Artmayer for the histology analysis, Alicia Emley for the color photography, Bradley Jarrold and Pam Groen for immunohistochemical staining, and Drs. Patric Tso and Vicky Ng for helping in the quantitative tissue lipid analysis. This work was partially supported by grants from the National Institutes of Health (DK 54930 to H.D.). Additional support was provided by the Children's Hospital Research Foundation.

Manuscript received 5 June 2000 and in revised form 14 November 2000.

REFERENCES

1. Brown, M. S., K. Luskey, H. A. Bohmfalk, J. Helgeson, and J. L. Goldstein. 1976. Role of the LDL receptor in the regulation of cholesterol and lipoprotein metabolism. *In* Lipoprotein Metabolism. H. Greten, editor. Springer, Berlin. 82–89.
2. Kowal, R. C., J. Herz, J. L. Goldstein, V. Esser, and M. S. Brown. 1989. Low density lipoprotein receptor-related protein mediates uptake of cholesteryl esters derived from apolipoprotein E-enriched lipoproteins. *Proc. Natl. Acad. Sci. USA.* **86:** 5810–5814.
3. Kowal, R. C., J. Herz, K. H. Weisgraber, R. W. Mahley, M. S. Brown, and J. L. Goldstein. 1990. Opposing effects of apolipoproteins E and C on lipoprotein binding to low density lipoprotein receptor-related protein. *J. Biol. Chem.* **265:** 10771–10779.
4. Strickland, D. K., J. D. Ashcom, S. Williams, W. H. Burgess, M. Migliorini, and W. S. Argraves. 1990. Sequence identity between the alpha 2-macroglobulin receptor and low density lipoprotein receptor-related protein suggests that this molecule is a multifunctional receptor. *J. Biol. Chem.* **265:** 17401–17404.
5. Assmann, G., and U. Seedorf. 1995. Acid Lipase Deficiency: Wolman Disease and Cholesteryl Ester Storage Disease. McGraw-Hill, New York.
6. Du, H., D. P. Witte, and G. A. Grabowski. 1996. Tissue and cellular specific expression of murine lysosomal acid lipase mRNA and protein. *J. Lipid Res.* **37:** 937–949.
7. Nakagawa, H., S. Matsubara, M. Kuriyama, H. Yoshidome, J. Fujiyama, H. Yoshida, and M. Osame. 1995. Cloning of rat lysosomal acid lipase cDNA and identification of the mutation in the rat model of Wolman's disease. *J. Lipid Res.* **36:** 2212–2218.
8. Du, H., M. Duanmu, and L. R. Rosa. 1998. Mouse lysosomal acid lipase: characterization of the gene and analysis of promoter activity. *Gene.* **208:** 285–295.
9. Anderson, R. A., R. S. Byrum, P. M. Coates, and G. N. Sando. 1994. Mutations at the lysosomal acid cholesteryl ester hydrolase gene locus in Wolman disease. *Proc. Natl. Acad. Sci. USA.* **91:** 2718–2722.
10. Anderson, R. A., N. Rao, R. S. Byrum, C. B. Rothschild, D. W. Bowden, R. Hayworth, and M. Pettenati. 1993. In situ localization of the genetic locus encoding the lysosomal acid lipase/cholesteryl esterase (LIPA) deficient in Wolman disease to chromosome 10q23.2-q23.3. *Genomics.* **15:** 245–247.
11. Du, H., M. Duanmu, D. Witte, and G. A. Grabowski. 1998. Targeted disruption of the mouse lysosomal acid lipase gene: long-term survival with massive cholesteryl ester and triglyceride storage. *Hum. Mol. Genet.* **7:** 1347–1354.
12. Gerdes, L. U., C. Gerdes, I. C. Klausen, and O. Faegeman. 1992. Generation of analytic plasma lipoprotein profiles using prepacked superose 6B columns. *Clin. Chim. Acta.* **205:** 1–9.
13. Gordon, S., L. Lawson, S. Rabinowitz, P. R. Crocker, L. Morris, and V. H. Perry. 1992. Antigen markers of macrophage differentiation in murine tissues. *Curr. Top. Microbiol. Immunol.* **181:** 1–37.

14. Folch, J., M. Lees, and G. H. S. Stanley. 1957. A simple method for the isolation and purification of total lipids from animal tissues. *J. Biol. Chem.* **125:** 497–509.
15. Biggs, H. G., J. M. Erikson, and W. R. Moorehead. 1975. A manual colorimetric assay of triglycerides in serum. *Clin. Chem.* **21:** 437–441.
16. Rudel, L. L., and M. D. Morris. 1973. Determination of cholesterol using o-phthalaldehyde. *J. Lipid Res.* **14:** 164–166.
17. Spiegeman, B. M., and J. S. Flier. 1996. Adipogenesis and obesity: rounding out the big picture. *Cell.* **87:** 377–389.
18. Kuriwaki, K., and H. Yoshida. 1999. Morphological characteristics of lipid accumulation in liver-constituting cells of acid lipase deficiency rats (Wolman's disease model rats). [In Process Citation] *Pathol. Int.* **49:** 291–297.
19. Daly, T. M., C. Vogler, B. Levy, M. E. Haskins, and M. S. Sands. 1999. Neonatal gene transfer leads to widespread correction of pathology in a murine model of lysosomal storage disease. *Proc. Natl. Acad. Sci. USA.* **96:** 2296–2300.
20. Heur, M., H. Du, D. Witte, and G. A. Grabowski. 2000. Model for Kupffer cell proliferation in lysosomal acid lipase deficient mice. *Am. J. Hum. Gent.* **67:** 1575 (Abstract).
21. Li, A. C., F. R. B. Guidez, J. G. Collier, and C. K. Glass. 1998. The macrosialin promoter directs high levels of transcriptional activity in macrophages dependent on combinatorial interactions between PU.1 and c-Jun. *J. Biol. Chem.* **273:** 5389–5399.
22. Naito, M., G. Hasegawa, and K. Takahashi. 1997. Development, differentiation, and maturation of Kupffer cells. *Microsc. Res. & Tech.* **39:** 350–364.
23. Shimomura, I., R. E. Hammer, J. A. Richardson, S. Ikemoto, Y. Bashmakov, J. L. Goldstein, and M. S. Brown. 1998. Insulin resistance and diabetes mellitus in transgenic mice expressing nuclear SREBP-1c in adipose tissue: model for congenital generalized lipodystrophy. *Genes Dev.* **12:** 3182–3194.
24. Peet, D. J., S. D. Turley, W. Ma, B. A. Janowski, J. M. Lobaccaro, R. E. Hammer, and D. J. Mangelsdorf. 1998. Cholesterol and bile acid metabolism are impaired in mice lacking the nuclear oxysterol receptor LXR alpha. *Cell.* **93:** 693–704.
25. Barak, Y., M. C. Nelson, E. S. Ong, Y. Z. Jones, P. Ruiz-Lozano, K. R. Chien, A. Koder, and R. M. Evans. 1999. PPAR gamma is required for placental, cardiac, and adipose tissue development. *Mol. Cell.* **4:** 585–595.
26. Brown, M. S., and J. L. Goldstein. 1998. Sterol regulatory element binding proteins (SREBPs): controllers of lipid synthesis and cellular uptake. *Nutr. Rev.* **56:** S1–S3, S54–S75.
27. Gasic, G. P. 1994. Basic-helix-loop-helix transcription factor and sterol sensor in a single membrane-bound molecule [comment]. *Cell.* **77:** 17–19.
28. Janowski, B. A., P. J. Willy, T. R. Devi, J. R. Falck, and D. J. Mangelsdorf. 1996. An oxysterol signalling pathway mediated by the nuclear receptor LXR alpha. *Nature.* **383:** 728–731.
29. Nagy, L., P. Tontonoz, J. G. Alvarez, H. Chen, and R. M. Evans. 1998. Oxidized LDL regulates macrophage gene expression through ligand activation of PPARγ. *Cell.* **93:** 229–240.
30. Forman, B. M., P. Tontonoz, J. Chen, R. P. Brun, B. M. Spiegelman, and R. M. Evans. 1995. 15-Deoxy-delta 12, 14-prostaglandin J2 is a ligand for the adipocyte determination factor PPAR gamma. *Cell.* **83:** 803–812.
31. Kopecky, J., G. Clarke, S. Enerback, B. Spiegelman, and L. P. Kozak. 1995. Expression of the mitochondrial uncoupling protein gene from the aP2 gene promoter prevent genetic obesity. *J. Clin. Invest.* **96:** 2914–2923.
32. Soloveva, V., R. A. Graves, M. M. Rasenick, B. M. Spiegelman, and S. R. Ross. 1997. Transgenic mice overexpressing the beta 1-adrenergic receptor in adipose tissue are resistant to obesity. *Mol. Endocrinol.* **11:** 27–38.
33. Wang, N., M. J. Finegold, A. Bradley, C. N. Ou, S. V. Abdelsayed, M. D. Wilde, L. R. Taylor, D. R. Wilson, and G. J. Darlington. 1995. Impaired energy homeostasis in C/EBPα knockout mice. *Science.* **269:** 1108–1112.
34. Katz, E. B., A. E. Stenbit, K. Hatton, R. DePinho, and M. J. Charron. 1995. Cardiac and adipose tissue abnormalities but not diabetes in mice deficient in GLUT4. *Nature.* **377:** 151–155.
35. Cummings, D. E., E. P. Brandon, J. V. Planas, K. Motamed, R. L. Idzerda, and G. S. McKnight. 1996. Genetically lean mice result from targeted disruption of the RIIβ subunit of protein kinase A. *Nature.* **382:** 622–626.